ChemComm

Gold nanoparticle as an outstanding catalyst for the hydrogen evolution reaction

Journal:	*ChemComm*
Manuscript ID	CC-COM-01-2018-000038.R1
Article Type:	Communication

Journal Name

COMMUNICATION

Gold nanoparticle as an outstanding catalyst for the hydrogen evolution reaction

Received 00th January 20xx,
Accepted 00th January 20xx

DOI: 10.1039/x0xx00000x

www.rsc.org/

Tien D. Tran,[a] Mai T.T. Nguyen,[b*] Hoang V. Le,[a] Duc N. Nguyen,[a] Quang Duc Truong,[c] Phong D. Tran[a,d*]

Electrode made of Au nanoparticles, ca. 13 nm in diameter, displays outstanding catalytic activity for the hydrogen evolution reaction in water. At 200 mV overpotential, it operates with a catalytic rate TOFs of 0.3 s^{-1}, just being among the best performances ever achieved for a Pt-free H_2-evolving catalyst.

Water (photo)electrolysis represents an attractive technology for large scale production of hydrogen that is subsequently used as a clean fuel. Due to its slow kinetic, a dual of efficient catalysts for the hydrogen evolution reaction (HER) and the oxygen evolution reaction (OER) is required to accelerate the water electrolysis process. Pt remains as the best catalyst for the HER. However, its limit storage on the earth`s crust raises question on its application for a large scale H_2 production. In this context, several families of catalysts including metal, metal alloys, chacolgenides of transition metals, phosphides of transition metals and coordination complexes of transition metals have been investigated as alternatives to Pt catalyst.[1, 2] Au was considered as a poor catalyst because the theoretical calculation showed a week adsorption of hydrogen atoms on the Au catalyst surface.[3] Therefore, Au is an electrode support of choice for loading HER catalysts in their activity assay. The choice is more "judicious" for the catalysts made of the sulfides of transition metals. That is because Au displays an outstanding electrical conductivity and a strong chemical interaction with sulfide ligands. Furthermore, metal sulfide nanosheets, like MoS_2 nanosheets, with controlled morphology can be directly grown on an Au substrate.[4-6] However, recent theoretical studies revealed Au as a non-innocent electrode support that offered a positive effect to MoS_2[7, 8] and $[Mo_3S_{13}]^{2-}$ [ref.9] catalysts by lowering the hydrogen adsorption free Gibbs energy. As a consequence, using an Au disk electrode helped to improve the catalytic activity of these catalysts. For example, under the same applied potential, a $[Mo_3S_{13}]^{2-}$/Au electrode operated at a catalytic rate of about three fold faster than that achieved for a $[Mo_3S_{13}]^{2-}$/ glassy carbon electrode (at overpotential of 200 mV, the TOFs were determined to be 0.35 and 0.11 s^{-1}).[9]

Other than the Au flat electrode support, Au nanoparticles (hereafter denoted as Au-NPs) could also alter the activity of HER catalysts. It has been demonstrated that a decoration of Au-NPs onto MoS_2,[10] Mo_2N[11] catalysts induced a significant enhancement of activity. Apparently, altering the hydrogen adsorption free Gibbs energy on these catalysts thanks to the presence of Au-NPs was a reason behind the activity enhancement.[8] For the case of MoS_2 catalyst, the presence of Au-NPs may also improve the charge transport between the adjacent MoS_2 layers.[10] That definitively contributed to the superior catalytic activity observed. However, Au planar disk and Au-NPs were still considered to be catalytically inactive or to display just low activity.

In this report, we show that Au-NPs itself is an outstanding HER catalyst in an acidic solution. It is also active in near-to-neutral or neutral pH solutions. Au-NPs with small size of 13 nm, hereafter denoted as Au-NPs-13nm, even displays higher catalytic activity compared with the top most active MoS_2 catalysts. The key for its high activity is the capability to renew its surface by completely removing the adsorbed surfactant during the H_2-evolving operation. Indeed, the surfactant like citrate was usually used to drive the growth of Au NPs in solution synthesis.

We prepared Au-NPs-13nm following the method described by Turkevich et al[12] using $HAuCl_4$ and sodium citrate. A deep wine red solution of Au-NPs in water showing a plasmonic excitation peak at ca. 521 nm was obtained (**figure S1**). We then drop-casted this solution onto a clean fluorine-doped tin oxide (FTO) substrate or a copper grid for microscopic and spectroscopic analyses. Transition Electron Microscopic analysis confirmed a homogeneous morphology of the resultant Au-NPs having

[a] Department of Advanced Materials Science and Nanotechnology, University of Science and Technology of Hanoi, Vietnam Academy of Science and Technology, 18 Hoang Quoc Viet, Ha Noi, Viet Nam. Email: tran-dinh.phong@usth.edu.vn
[b] School of Chemical Engineering, Hanoi University of Science and Technology, 1 Dai Co Viet road, Ha Noi, Viet Nam. Email: nguyenthituyetmai87@gmail.com
[c] Institute of Multidisciplinary Research for Advanced Materials, Tohoku University, Sendai 980-8577, Japan
[d] Department of Chemistry, College of Natural Sciences, Hanyang University, Seoul 04763, Republic of Korea. Email: trandp@hanyang.ac.kr
Electronic Supplementary Information (ESI) available: [details of any supplementary information available should be included here]. See DOI: 10.1039/x0xx00000x

spherical shape with an average diameter size of ca. 13 nm (**figure 1a**). Powder X-ray diffraction analysis revealed the polycrystalline structure with (111) and (022) faces (**figure S2**). ATR-IR analysis evidenced the presence of the citrate ligand on the surface of Au-NPs with the characteristic ν(C=O) stretching vibration at 1570 cm^{-1} (**figure 1c**, black trace).[13] The presence of the citrate ligand was further confirmed by X-ray photoelectron spectroscopic (XPS) analysis. The characteristic C1s signature of the C=O group was found at binding energy of 288.2 eV (**figure 1d**, blue trace).[14] Signature at lower binding energy of 284.6 eV is attributed to the C within the alkyl chain and to the C residual. Carboxylic O1s core level was observed at 535.4 eV (**figure 1e**, blue trace).[15] Interestingly, $Au4f_{7/2}$ was found at 83.1 eV representing a clear shift to lower binding energy compared with the same signature reported for a pure metallic Au (**figure 1f**, blue trace).[16] We attribute this shift to the negative charge on Au-NPs surface provided by the citrate ligand. Removal of this anionic ligand recovers the metallic surface that causes a shift to higher binding energy of the Au4f core level (*see following section*).

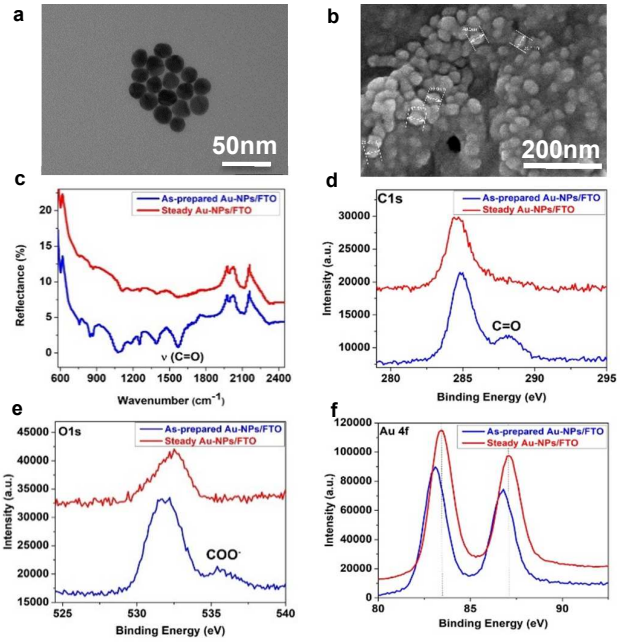

Figure 1. ***(a)*** *TEM image of Au-NPs-13nm;* ***(b)*** *SEM image of a 350μg-*Au-NPs-13nm/FTO *electrode;* ***(c)*** *ATR-IR spectra and* ***(d-f)*** *XPS spectra collected on the 350μg-*Au-NPs-13nm/FTO *electrode when it was freshly prepared (blue traces) and after its steady catalytic activity was achieved (red traces)*

We then assayed the H_2-evolving activity of Au-NPs-13nm in a pH 0 H_2SO_4 electrolyte solution. To do so, 50 μL of the Au-NPs-13nm solution was drop-casted onto a FTO electrode having a working area of 0.28 cm^2. Assuming the $HAuCl_4$-to-Au-NPs conversion yield is unity, this volume loading corresponds to a catalyst weight loading of 70 μg Au-NPs over 1 cm^2. Hereafter, for seeking of clarification, we refer the resultant electrode as 70μg-Au-NPs-13nm/FTO. Prior to use, the resultant electrode was first dried naturally in air and then in a vacuum oven heated at 40°C. SEM analysis conducted on this electrode revealed the aggregation of Au NPs into larger particles of ca. 35-40 nm in diameter (**figure 1b**). The as prepared 70μg-Au-NPs-13nm/FTO electrode displayed a reasonable catalytic activity with an onset overpotential of ca. 150 mV. This electrode required ca. 320 mV of overpotential to generate a catalytic current of 5.0 $mA.cm^{-2}$ (**figure 2a**, olive curve). However, repeating potential polarization from the open circuit voltage, *e.g.* +0.2V *vs.* RHE, to a cathodic potential of -0.3V *vs.* RHE with a potential scan rate of 2 $mV.s^{-1}$ induced a significant enhancement of the catalytic activity. The steady 70μg-Au-NPs-13nm/FTO electrode, obtained by repeating five potential polarizations, showed a small onset overpotential of ca. 100 mV and required an overpotential of ca. 250 mV to generate 10 $mA.cm^{-2}$ (**figure 2a**, blue curve). Without an iR correction, a Tafel slop value of 70 $mV.decade^{-1}$ was deduced. Control experiment with a clean FTO electrode showed negligible cathodic current in the same potential range **(figure 2a**, black dash curve). Small catalytic current of 0.2 mA/cm^2 was obtained for a clean, steady Au disk electrode at overpotential of 250 mV, representing two orders of magnitude lower catalytic activity compared with the 70μg-Au-NPs/FTO electrode (**figure 2a**, red curve; *see also* ***figure S3*** *for smaller current scale*). These results clearly evidenced the specific catalytic activity of Au-NPs electrode.

When assaying for the 70μg-Au-NPs-13nm/FTO electrode, we observed a negligible capacitive current that indicated an effective electron transport within the electrode. Thus, phenomenon of slow electron transport within the bulk volume of a thick catalyst layer[17] was not an issue for the current electrode. We then investigated the catalytic activity in function of the Au-NPs catalyst loading. **Figure 2b** shows a linear increasing of the catalytic activity, represented by the catalytic current at -0.20 V *vs.* RHE, on the catalyst loading. The steady 350μg-Au-NPs-13nm/FTO electrode showed an outstanding activity. This electrode operated with just a moderate onset overpotential of 50 mV. To generate a current of 10 $mA.cm^{-2}$, this electrode required 180 mV overpotential (**figure 2a**, pink dash curve). At overpotential of 200 mV, the electrode generated a catalytic current of 11 $mA.cm^{-2}$. Thus, the lower limit catalytic rate TOFs was estimated to be 3.2 10^{-2} s^{-1} with an assumption that all Au atoms, meaning both the bulk and surface ones, are catalytically active. However, with an average effective size of 40 nm, the number of surface atoms over the total number of volume atoms is estimated to be 9.6%. Thus, the effective catalytic rate can be normalized to be 0.3 s^{-1}. This performance presents the Au-NPs-13nm as one of the best Pt-free HER catalysts, being comparable with the top MoS_2, $[Mo_3S_{13}]^{2-}$ cluster or metal phosphide (**Table S1**). However, Au-NPs-13nm is still less active compared with Pt nanoparticle that generates a catalytic rate of 0.9 s^{-1} at zero overpotential.[4]

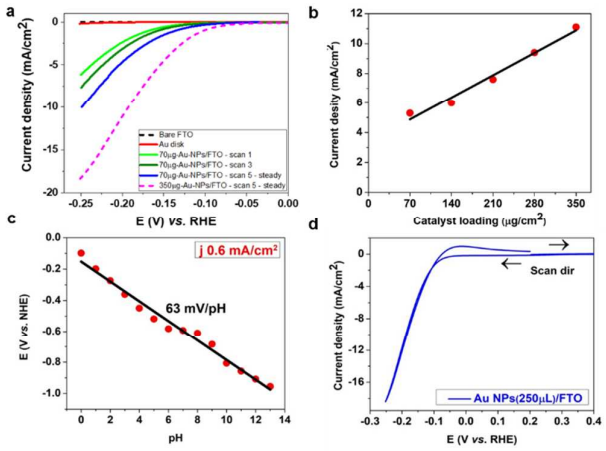

Figure 2. ***(a)*** *I-V curves recorded on the Au-NPs-13nm/FTO electrodes having different catalyst loadings;* ***(b)*** *Catalytic current at applied potential of -0.2V vs. RHE in function of the catalyst loading;* ***(c)*** *pH titration at a catalytic current of 0.6 mA.cm^{-2}; and* ***(d)*** *Cyclic voltammogram recorded on a steady 350µg-Au-NPs-13nm/FTO electrode*

Volmer reaction: $Au + H^+ + e^- \leftrightarrow Au - H$
Heyrovsky reaction: $Au - H + H^+ + e^- \leftrightarrow Au - H_2$
Tafel reaction: $2\,Au - H \leftrightarrow Au - H_2$

The Tafel slope was calculated to be 60 mV.decade^{-1}, indicating either a Heyrovsky or a Tafel rate determining step.[18] We found that in order to keep generating a catalytic current of 0.6 mA.cm^{-2}, 63 mV was needed to add to the applied potential when pH of the electrolyte was increased by one unity (**figure 2c**). It suggests the involvement of $1H^+$ and $1e^-$ in the rate limiting step.[19] Furthermore, the H_2 evolution rate on an Au-NPs loaded carbon rotating disk increased with the creasing of rotating rate (**figure S4**). This result confirms the mass diffusion of proton as a limitation of the reaction. Putting together these results, we conclude the Heyrovsky discharge reaction as the rate determining step for the H_2-evolution on Au-NPs catalyst.

Table 1. Steady catalytic activity of a *350µg*-Au-NPs-13nm/FTO *electrode* with and without the presence of an organic adsorbate on the surface of Au NPs(*)

	Citrate	L-cysteine	MSA	bipyr	terpyr	CTAB
Presence of adsorbate	2.1	2.6	1.4	1.8	4.2	4.0
Removal of adsorbate	11.0	11.0	8.9	9.0	8.3	9.0

(*) Catalytic current was measured at applied potential of -0.2V vs. RHE. Electrolyte was a pH 0 H_2SO_4 solution

In order to identify the potential reasons behind the significant enhancement of catalytic activity observed, we conducted microscopic and spectroscopic analyses on the steady 350µg-Au-NPs-13nm/FTO electrode. Prior to use for characterization, the electrode was carefully washed with DI water to remove all physio-adsorbed species and then dried in vacuum. SEM analysis showed similar morphology to that observed for an as-prepared electrode (**figure S5**). However, a clear change in surface chemistry was observed. ATR-IR analysis revealed the disappearance of the ν(C=O) vibration (**figure 1c**, *red trace*). In the XPS analysis, the characteristic C1s and O1s core level signatures of the C=O group were disappeared (**figures 1d, 1e**). These results clearly confirm the removal of the citrate ligand from the Au-NPs surface. The removal of the anionic ligand neutralizes the surface charge on the Au-NPs. As a consequence, Au4f core level was shifted to higher binding energy (**figure 1f**, *red trace*). Indeed, $Au4f_{7/2}$ was found at 83.5 eV, being close to that determined for metallic Au.[16]

The displacement of citrate ligand could be due to the generation of hydride species on Au surface during the H_2-evolving process. Indeed, hydride was found to have the highest binding energy with Au-NPs among different surface adsorbates including thiolate, I^- and Br^- anions as well as PVP polymer. Therefore, when the hydride species was produced, it replaces these adsorbates.[20] This hypothesis was further supported by the appearance of an oxidative event at potential of 0 V *vs.* RHE (**figure 2d**). This event was obvious for the Au-NPs-13nm/FTO electrode with high catalyst loading, thus providing a significant H_2-evolving rate at a cathodic potential. We attributed this event to the re-oxidation of adsorbed hydrogen species on the Au-NPs. Brust and Gordillo demonstrated a reversible reductive generation/ oxidative re-oxidation of Au-H_2 species at an equilibrium potential of -0.22 V *vs.* NHE (the measurement was conducted with an electrode made of Au-NPs absorbed on Hg drop and in an acetate pH 4.5 electrolyte).[21] Furthermore, the redox event was determined to involve $1H^+$ and $1e^-$. Therefore, we can deduce a potential of ca. +0.04 *vs.* NHE for the redox event in a pH 0 electrolyte solution. This potential is very close to the value we observed for the oxidation event.

We found that not only a citrate anionic ligand blocks the active surface of Au-NPs, thus lowers the catalytic activity, but also other anionic ligands like L-cysteine, methanesulfonic acid (MSA), cationic ligands like hexadecyl trimethylammonium bromide (CTAB) or neutral ligand like bipyridine (bipyr) or terpyridine (terpyr). When the 350µg-Au-NPs-13nm/FTO electrode had already achieved its steady activity, we immersed this electrode in a solution containing one of the above surfactants (*See supporting information for more details*). ATR-IR analysis clearly evidenced the adsorption of these surfactants on the Au-NPs surface. The presence of these surfactants significantly reduced the activity of the 350µg-Au-NPs/FTO electrode (**Table 1**). However, being similar to the case of citrate surfactant described this above, repeating the cathodic potential polarization progressively recovered the initial activity of the 350µg-Au-NPs/FTO electrode. The activity recovering is accompanied with the removal of surfactant/ ligand from the surface of Au-NPs (**figure S6**).

We were next interested in investigating the impacts of Au particle size on its catalytic activity. Au-NPs sized of ca. 60 nm (**figure S7**), denoted as Au-NPs-60nm, was synthesized by adapting the seeded growth synthesis described by Bastus *et al.*[22] Au-NPs-60nm/FTO electrode showed similar electrochemical property to that observed for the Au-NPs-13nm/FTO electrode, namely significant enhancement of its catalytic activity upon the complete removal of citrate adsorbate by repeating the potential polarization. However, due to its small surface area, Au-NPs-60nm showed lower catalytic

current compared with Au-NPs-13nm analogue at a given applied potential (**figure S8**).

Conclusions

To conclude, we have demonstrated that Au-NPs is one of the best Pt-free HER catalysts ever reported. The key to Au-NPs activity is its clean surface being free of any adsorbates. Interestingly, the adsorbates, *e.g.* incorporated during the synthesis of Au-NPs, can be easily removed by repeating the cathodic potential polarization on the Au-NPs. Therefore Au-NPs could be considered as an attractive alternative to Pt catalyst for engineering a photoelectrode for PEC device for the solar H_2 generation.

Conflicts of interest

There are no conflicts to declare

Acknowledgment

Phong D. Tran, Tien D. Tran, Hoang V. Le and Duc N. Nguyen acknowledge the Office of Naval Research Global for funding support through the project N62909-16-1-2191. Mai T.T. Nguyen acknowledges the National Foundation for Science and Technology Development (NAFOSTED) for funding support through the project: 103.02-2016.24. The authors also would like to thank T.D.N. Ha (ITODYS, University Paris-Diderot, France) for the XRD and TEM measurements.

References

1. I. Roger, M. A. Shipman and M. D. Symes, *Nat. Rev. Chem.* , 2017, **1**, 0003.
2. S. Fukuzumi, Y.-M. Lee and W. Nam, *Coord. Chem. Rev.*, 2018, **355**, 54-73.
3. B. Hinnemann, P. G. Moses, J. Bonde, K. P. Jørgensen, J. H. Nielsen, S. Horch, I. Chorkendorff and J. K. Nørskov, *J. Am. Chem. Soc.*, 2005, **127**, 5308-5309.
4. T. F. Jaramillo, K. P. Jørgensen, J. Bonde, J. H. Nielsen, S. Horch and I. Chorkendorff, *Science*, 2007, **317**, 100-102.
5. S. Chatterjee, K. Sengupta, S. Dey and A. Dey, *Inorg. Chem.* , 2013, **52**, 14168-14177.
6. C. Tsai, H. Li, S. Park, J. Park, H. S. Han, J. K. Nørskov, X. Zheng and F. Abild-Pedersen, *Nat. Commun.* , 2017, **8**, 15113.
7. C. Ling, Y. Ouyang, L. Shi, S. Yuan, Q. Chen and J. Wang, *ACS Catal.*, 2017, **7**, 5097-5102.
8. C. Tsai, F. Abild-Pedersen and J. K. Nørskov, *Nano Lett.*, 2014, **14**, 1381-1387.
9. T. R. Hellstern, J. Kibsgaard, C. Tsai, D. W. Palm, L. A. King, F. Abild-Pedersen and T. F. Jaramillo, *ACS Catal.* , 2017, **7**, 7126-7130.
10. J. Kim, S. Byun, A. J. Smith, J. Yu and J. Huang, *J. Phys. Chem. Lett.*, 2013, **4**, 1227-1232.
11. U. Joshi, J. Lee, C. Giordano, S. Malkhandi and B. S. Yeo, *Phys. Chem. Chem. Phys.*, 2016, **18**, 21548-21553.
12. J. Turkevich, P. C. Stevenson and J. Hillier, *Disc. Faraday Soc.* , 1951, **11**, 55-75.
13. S. Lou, J.-y. Ye, K.-q. Li and A. Wu, *Analyst*, 2012, **137**, 1174-1181.
14. L. Ge, X. Jing, J. Wang, J. Wang, S. Jamil, Q. Liu, F. Liu and M. Zhang, *J. Mater. Chem.* , 2011, **21**, 10750-10754.
15. F. Bournel, C. Laffon, P. Parent and G. Tourillon, *Surf. Sci.* , 1996, **350**, 60-78.
16. J. C. Fuggle, E. Källne, L. M. Watson and D. J. Fabian, *Phys. Rev. B*, 1977, **16**, 750-761.
17. H. Vrubel, T. Moehl, M. Gratzel and X. Hu, *Chem. Commun.* , 2013, **49**, 8985-8987.
18. A. Kahyarian, B. Brown and S. Nesic, *J. Electrochem. Soc.* , 2017, **164**, H365-H374.
19. C. Costentin, M. Robert and J.-M. Savéant, *Chem. Rev.*, 2010, **110**, PR1-PR40.
20. S. M. Ansar, F. S. Ameer, W. Hu, S. Zou, C. U. Pittman and D. Zhang, *Nano Lett.*, 2013, **13**, 1226-1229.
21. M. Brust and G. J. Gordillo, *J. Am. Chem. Soc.* , 2012, **134**, 3318-3321.
22. N. G. Bastús, J. Comenge and V. Puntes, *Langmuir*, 2011, **27**, 11098-11105.